Remote Sensing of Environment 139 (2013) 291–305

Contents lists available at ScienceDirect

Remote Sensing of Environment

journal homepage: www.elsevier.com/locate/rse

Hyperspectral *versus* multispectral crop-productivity modeling and type discrimination for the HyspIRI mission

Isabella Mariotto [a,b,*], Prasad S. Thenkabail [b], Alfredo Huete [c], E. Terrence Slonecker [d], Alexander Platonov [e]

[a] Soil, Water & Environmental Science Department, The University of Arizona, USA
[b] U.S. Geological Survey, Flagstaff Science Center, Flagstaff, AZ 86001, USA
[c] Plant Functional Biology and Climate Change, University of Technology Sydney, Australia
[d] U.S. Geological Survey, Eastern Geographic Science Center, Reston, VA, USA
[e] International Water Management Institute (IWMI), Tashkent Office, Uzbekistan

ARTICLE INFO

Article history:
Received 30 April 2012
Received in revised form 16 July 2013
Accepted 3 August 2013
Available online 7 September 2013

Keywords:
Hyperspectral
Multispectral
Hyperion
HyspIRI
Biomass
Crop type
Vegetation indices
Narrowband
Broadband

ABSTRACT

Precise monitoring of agricultural crop biomass and yield quantities is critical for crop production management and prediction. The goal of this study was to compare hyperspectral narrowband (HNB) *versus* multispectral broadband (MBB) reflectance data in studying irrigated cropland characteristics of five leading world crops (cotton, wheat, maize, rice, and alfalfa) with the objectives of: 1. Modeling crop productivity, and 2. Discriminating crop types. HNB data were obtained from Hyperion hyperspectral imager and field ASD spectroradiometer, and MBB data were obtained from five broadband sensors: Landsat-7 Enhanced Thematic Mapper Plus (ETM+), Advanced Land Imager (ALI), Indian Remote Sensing (IRS), IKONOS, and QuickBird. A large collection of field spectral and biophysical variables were gathered for the 5 crops in Central Asia throughout the growing seasons of 2006 and 2007. Overall, the HNB and hyperspectral vegetation index (HVI) crop biophysical models explained about 25% greater variability when compared with corresponding MBB models. Typically, 3 to 7 HNBs, in multiple linear regression models of a given crop variable, explained more than 93% of variability in crop models. The evaluation of λ_1 (400–2500 nm) *versus* λ_2 (400–2500 nm) plots of various crop biophysical variables showed that the best two-band normalized difference HVIs involved HNBs centered at: (i) 742 nm and 1175 nm (HVI742-1175), (ii) 1296 nm and 1054 nm (HVI1296-1054), (iii) 1225 nm and 697 nm (HVI1225-697), and (iv) 702 nm and 1104 nm (HVI702-1104). Among the most frequently occurring HNBs in various crop biophysical models, 74% were located in the 1051–2331 nm spectral range, followed by 10% in the moisture sensitive 970 nm, 6% in the red and red-edge (630–752 nm), and the remaining 10% distributed between blue (400–500 nm), green (501–600 nm), and NIR (760–900 nm).
Discriminant models, used for discriminating 3 or 4 or 5 crop types, showed significantly higher accuracies when using HNBs (>90%) over MBBs data (varied between 45 and 84%).
Finally, the study highlighted 29 HNBs of Hyperion that are optimal in the study of agricultural crops and potentially significant to the upcoming NASA HyspIRI mission. Determining optimal and redundant bands for a given application will help overcoming the Hughes' phenomenon (or curse of high dimensionality of data).

1. Introduction

Accurate quantification of agricultural biophysical parameters is critical for effective and sustainable cropland management operations. Precise monitoring of biophysical quantities, specifically biomass (kg\m^2) and grain yield (ton/ha), allows farmers to optimize crop productivity (productivity per unit of land; kg\m^2) and adopt best farm management practices. It is now widely accepted that remote sensing data, methods, and approaches provide the best options for large area agricultural cropland characterization as well as information needed for precision agricultural management practices by accurately mapping and pinpointing factors such as higher and lower biomass and yield levels within and between farm fields (Alchanatis & Cohen, 2011; Moran, Inoue, & Barnes, 1997; Thenkabail, 2003).

Nevertheless, traditional multispectral broadband sensor data have known limitations of sensor saturation (Thenkabail, Enclona, Ashton, Legg, & De Dieu, 2004; Thenkabail, Enclona, Ashton, & Van Der Meer, 2004; Thenkabail, Smith, & De-Pauw, 2000), and absence of specific narrowbands to target and highlight specific biophysical and biochemical parameters (Gitelson, 2011; Gitelson, Gritz, & Merzlyak, 2003). These factors lead to significant uncertainties in spectro-biophysical and\or biochemical modeling of agricultural crops. The need of targeting specific narrowbands to study the spectral properties of vegetation is obvious

* Corresponding author at: University of Texas at El Paso, Department of Geological Sciences, El Paso, TX 79968, USA. Tel. +1 575-635-5838.
E-mail address: is.mariotto@gmail.com (I. Mariotto).

0034-4257/$ – see front matter © 2013 Elsevier Inc. All rights reserved.
http://dx.doi.org/10.1016/j.rse.2013.08.002

given that the molecular composition of the plant material reflects, absorbs, and emits electromagnetic energy at specific wavelengths and with distinct patterns. Detecting accurate spectral information of vegetation as a result of different combinations of types and quantities of plant pigments (*e.g.*, chlorophyll-*a* and -*b*, carotenoids, and anthocyanins), leaf water content, live and senescent biomass, distribution of leaves, density of plants, as well as biophysical quantities such as biomass, leaf area index (LAI), plant height, and grain yield requires high spectral resolution (Asner, 1998; Govender, Dye, Weiersbye, Witkowski, & Ahmed, 2009; Hill, 2004).

Indeed, it has been shown how hyperspectral data can provide significant improvements in spectral information content when compared with broadbands in: (a) modeling biophysical and yield characteristics of agricultural crops (Thenkabail et al., 2000; Thenkabail, Smith, & De-Pauw, 2002), (b) measuring chlorophyll content of plants (Blackburn & Ferwerda, 2008), (c) sensing subtle variations in leaf pigment concentrations (Blackburn & Ferwerda, 2008), (d) extracting biochemical variables such as nitrogen and lignin (Houborg & Boegh, 2008), (e) detecting crop moisture variations (Colombo, Busetto, Meroni, Rossini, & Panigada, 2011), (f) assessing absolute water content in plant leaves (Jollineau & Howarth, 2008), (g) identifying small differences in percent green vegetation cover (Chen, Wang, & Wang, 2008), (h) detecting plant stress (Thenkabail, Enclona, Ashton and Van Der Meer, 2004), and (i) discriminating land-cover types (Thenkabail, Enclona, Ashton, Legg, et al., 2004). These studies have made significant advances in understanding, modeling, and mapping various biophysical and biochemical quantities of agricultural crops.

Nevertheless, the knowledge gap in fully exploiting hyperspectral narrowband data for agricultural cropland studies is still highly significant.

- First, extensive hyperspectral studies on crop spectral characteristics that utilize data from multiple dates, multiple seasons, multiple crops, and multiple sites from around the world are still required to build robust global models of various biophysical and biochemical parameters.
- Second, as a result of existing uncertainties that require richer datasets from various agroecosystems around the world, hyperspectral narrowbands (HNBs) and hyperspectral vegetation indices (HVIs) are still being explored to best model variability in various agricultural cropland quantities (Thenkabail, Lyon, & Huete, 2011).
- Third, it is widely accepted in various National Aeronautics and Space Administration's (NASA) Hyperspectral Infrared Imager (HyspIRI) workshops and symposia that comparative studies among hyperspectral and multispectral satellite data are required in various different applications, especially in studies pertaining to vegetation characterization, with the aim of advancing our understanding, modeling, and mapping of Earth's vegetation health and vegetation types using data in 10 nm narrow and contiguous wavebands over, for example, 380 to 2500 nm (HyspIRI ultra-violet to Short-Wave-Infrared wavelength).
- Fourth, the computational processing of hyperspectral data is still a challenge due to the massive data present for each pixel (hundreds of bands) (Varshney & Arora, 2004), and more insight on optimal wavebands is essential in reducing the high data dimension (Thenkabail et al., 2011); also, the number of redundant bands is often higher than the number of useful bands, which invariably leads to the Hughes' phenomenon (Thenkabail et al., 2011) and to large volumes of noisy data.
- Fifth, recent research has demonstrated that optimal information required to quantify crop biophysical characteristics is present in a few specific narrowbands (Chan & Paelinckx, 2008; Thenkabail, Enclona, Ashton, & Van Der Meer, 2004), and that Hyperion data located in specific portions of the spectrum can dramatically improve discrimination capabilities and classification accuracies for various agricultural crops, relative to broadbands such as Landsat Thematic Mapper (TM) and Système Pour l'Observation de la Terre (SPOT) High Resolution Visible (HRV) (Lee, Cohen, Kennedy, Maiersperger, & Gower, 2004; Thenkabail, Enclona, Ashton, Legg, et al., 2004).

Multiple studies worldwide are needed to firmly establish the optimal wavebands and to build effective understanding of the capabilities of these optimal HNBs and HVIs in agricultural crop characterization. This will allow developing an efficient timeframe of computational processing strategy for hyperspectral users in crop productivity and crop type mapping.

- Sixth, richer datasets from around the world will help build spectral libraries of agricultural crops, which are still in their infancy.

However, in hyperspectral data, the number of pure spectral signatures (endmembers) generally exceeds the real number present in a pixel, while in multispectral data the detectable number of endmembers is generally lower than the real number (Schaepman et al., 2009). This results in discussions about the use of the two technologies, and in the need of further comparison studies.

Given the above background, the goal of this study is to compare Hyperion and field spectroradiometer narrowband (400–2500 nm) data with the Enhanced Thematic Mapper (ETM+), Advanced Land Imager (ALI), Indian Remote Sensing Satellites (IRS), IKONOS, and QuickBird broadband data to study irrigated agriculture of 5 leading world crops: wheat, cotton, maize, rice, and alfalfa. Specific objectives were to: 1. model crop productivity and 2. discriminate crop types. The outcome of this research will help establish the optimal HNBs and HVIs that are best suited for modeling crop biophysical variables and crop types. The study is based on a large collection of *in-situ* field biological datasets collected during the 2006 and 2007 crop growing seasons over large-scale heavily irrigated areas of the arid Syr Darya river basin in Central Asia, where recent studies show that snowmelt water supplies from Himalayas are on swift decline.

2. Methods

2.1. Study area

The study was conducted in irrigated croplands of the Syr Darya river basin (SRB) in Uzbekistan, Central Asia. The SRB covers an area of 444,000 km^2 including parts of Uzbekistan, Kyrgyzstan, Tajikistan, and Kazakhstan (Fig. 1). It receives snowmelt runoff from the Himalayas, which is decreasing swiftly in recent years as a result of climate change (Geerken, Batikha, Celis, & DePauw, 2005). The annual diversion from SRB is almost equal to total annual inflow, which has serious ecological consequences for the Aral Sea. The climate is temperate continental and sub-continental with average temperature of 28–32 °C in July and 0–4 °C in January, and low precipitation of 100–200 mm/year mostly occurring from November to March. Data were collected in the Galaba and Kuva agricultural regions of Uzbekistan, which is one of the world's biggest producers of cotton. Other crops grown are maize, wheat, rice, and alfalfa—all major world crops. These 5 crops occupy about 50% of all cropland areas of the world (Thenkabail et al. 2012). The terrain is relatively flat ranging from 277 to 284 m in elevation in the Galaba farm, and from 464 to 470 m in the Kuva farm.

2.2. Hyperspectral and multispectral data characteristics

Hyperion hyperspectral imager on board the Earth Observing-1 (EO-1) satellite, multi-spectral Landsat-7 Enhanced Thematic Mapper Plus (ETM+), Advanced Land Imager (ALI), and RESEOURCESAT-1 (Indian Remote Sensing IRS-P6), and multispectral hyperspatial QuickBird and IKONOS satellite images were analyzed. The number of acquisitions and the characteristics of these images are shown in Table 1. Several thousand hyperspectral ASD Spectroradiometer data were consistently collected for each ground point location (at 1.2 m high Nadir 18° FOV) — at a spatial resolution of 0.1134 m and spectral

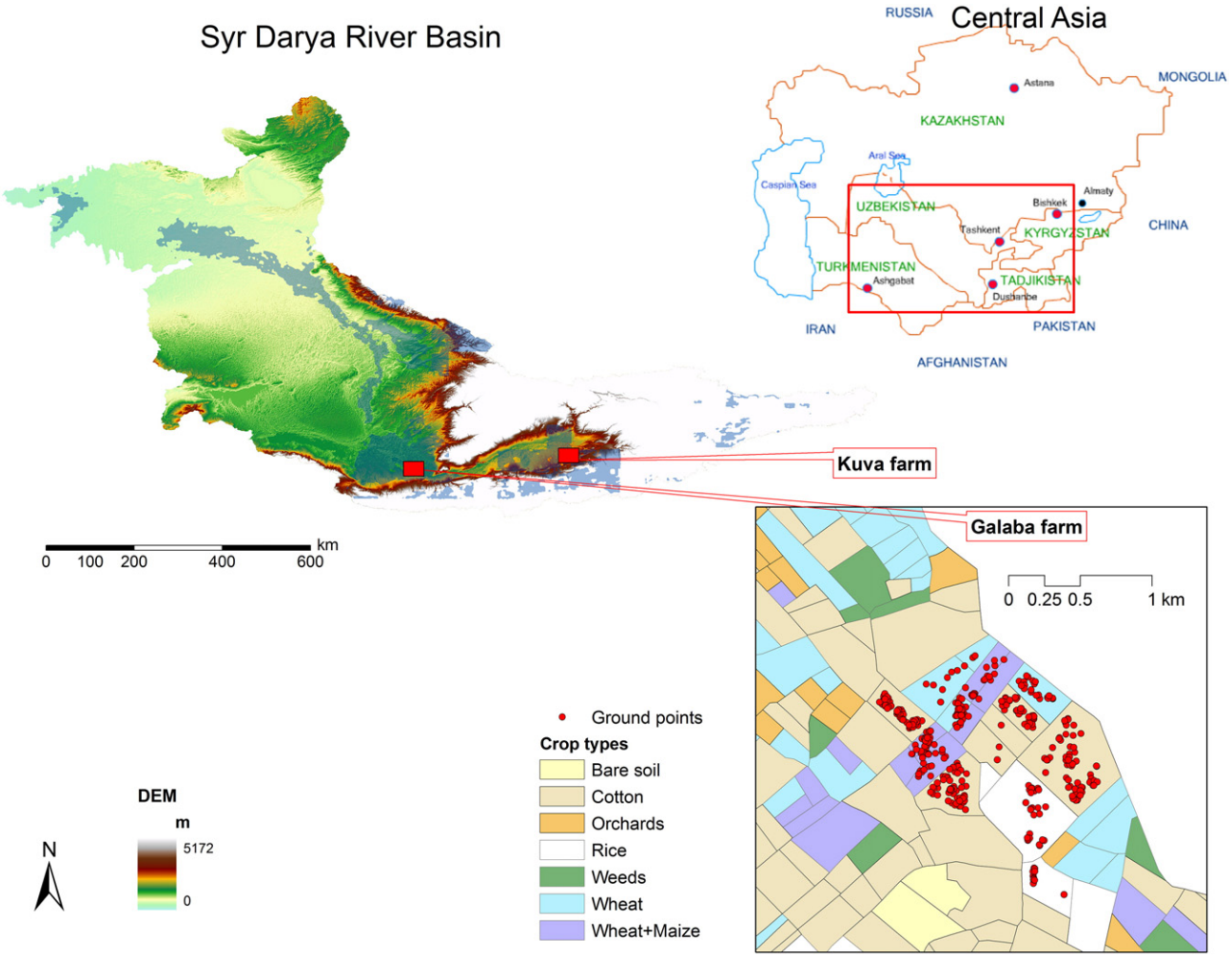

Fig. 1. Study area: Galaba and Kuva farm fields in the Syr Darya river basin, Central Asia. Crop types are shown for Galaba.

resolution of 1 nm from 400 to 2500 nm. Measurements were made for five crops – wheat, cotton, maize, rice, and alfalfa – in 59 different days (41 days in 2006 and 18 days in 2007) during the 2006 and 2007 crop growing seasons.

2.2.1. Image processing

In order to directly compare Hyperion, ETM+, ALI, IRS, IKONOS, and QuickBird sensors that have different radiometric resolutions, their respective digital numbers (DNs) were converted to absolute units of radiance (W m^{-2} sr^{-1} μm^{-1}), then to apparent at-satellite reflectance (%) (Thenkabail, Enclona, Ashton, Legg, et al., 2004; Thenkabail, Enclona, Ashton, & Van Der Meer, 2004; Thenkabail et al., 2002, 2011), and finally to surface reflectance (%) after atmospheric correction. Atmospheric correction was performed using the Fast Line-of-sight Atmospheric Analysis of Spectral Hypercubes (FLAASH) tool in ENVI 4.8 (Exelis Visual Information Solutions), which incorporates the MODTRAN4 radiation transfer code (Berk et al., 1999). All images were georectified and re-projected to a common UTM coordinate system and WGS84 datum.

Hyperion imagery consists of 242 contiguous spectral bands, of which only 198 are radiometrically calibrated (Beckmann & Mckinney, 2006). Among these 198 bands, the following 158 bands without any noise and free of atmospheric window effects were selected for this study: band 8 to 57 (426.82 nm to 925.41 nm), 79 to 119 (932.64 to 1336.15 nm), 133 to 164 (1477.43 nm to 1790.19 nm), 183 and 184 (1981.86–1991.96 nm), and 188 to 220 (2032.35 nm to 2355.21 nm) (Thenkabail, Enclona, Ashton, Legg, et al., 2004; Thenkabail, Enclona, Ashton, & Van Der Meer, 2004). Spectroradiometer wavelengths (1 nm) were averaged at 10 nm coincident to the band centers of the 158 Hyperion (10 nm width) selected bands. An example of spectroradiometer reflectance data for cotton is reported in Fig. 2. Reflectance values of the pixels intersecting the ground data points were extracted from each satellite image for each band using GIS.

2.3. Ground data

Field-plot data were collected for the five crops (wheat, cotton, maize, rice and alfalfa), throughout the summer crop growing seasons (April–October) of 2006 and 2007 every 15–20 days coincident with the field spectroradiometer measurement dates, and coincident – or maximum 1 day lapse – with the dates of the satellite overpass. Measurements were carried out in 1232 randomly chosen points scattered across farmers' plots (maize $n = 125$; wheat $n = 220$; rice $n = 37$; alfalfa $n = 57$; and cotton $n = 778$) (Fig. 1). At each point, GPS coordinates and crop type were recorded along with wet and dry biomass (kg/m^2), and/or yield (kg/m^2, or ton/ha). Biomass and yield were measured by samples cutting and weighting (for cotton yield, lint was measured) across all the study season. Canopy, soil, and weed covers were eye-estimated (%).

2.4. Crop productivity modeling using hyperspectral and multispectral data

Crop productivity models of biomass and yield are commonly computed either with a physically based approach or a statistical regression approach (Thenkabail et al., 2011). However, no single best approach is

Table 1
Characteristics of hyperspectral narrowband and multispectral broadband data used in this study.

Satellite/Sensor	Spatial resolution (m)	No. spectral bands used	Band range (nm)	Band width (nm)	Acquisition dates	Sample size
Hyperspectral						
Hyperion-EO1	30	158	400–2500	10	29/5/07, 01/8/07, 06/8/07	249
ASD-Spectroradiometer	0.1134 @1.2 m high NADIR view 18° FOV	158	400–2500	10 (averaged from 1 nm)	every 15–20 days May–Oct 2006, 2007	310
Multispectral						
Landsat 7 ETM+	30	6	450–2350	65–260	10/5/06, 11/6/06, 29/7/06, 14/8/06, 01/10/06	200
ALI-EO1	30	9	433–2350	19.79–270	01/8/07, 06/8/07	79
IRS(P6)-LISS3	23.5	4	520–1700	70–150	05/6/06, 15/6/06, 20/6/06, 09/7/06, 14/7/06, 26/8/06, 24/9/06, 27/10/06, 26/5/07, 19/6/07, 18/7/07, 30/8/07, 04/9/07	265
Hyperspatial						
QuickBird	2.44	4	450–900	70–140	26/7/06, 03/8/06	21
IKONOS	3.2	4	450–853	80–96	22/7/07	468

currently available to determine the optimal number of bands (Chen et al., 2008; Jollineau & Howarth, 2008). Therefore, models with rigorous search criterion or data mining are used in this study to determine optimal hyperspectral narrowband data involving hundreds of bands and thousands of vegetation indices (Thenkabail, Enclona, Ashton, Legg, et al., 2004; Thenkabail, Enclona, Ashton, & Van Der Meer, 2004; Thenkabail et al., 2000, 2002, 2011). Two different statistical approaches were adopted in this study to model crop biophysical models using HNBs as well as multispectral broadbands (MBBs): (a) stepwise multiple-linear regression models (SMRMs) (Hocking, 1976); and (b) correlation analyses (Glahn, 1968) between biomass or yield quantities and two-band vegetation indices (when hyperspectral data are involved, they will be referred to as HVIs because of the huge number of indices that are involved, see Section 2.4.2 for details; when multispectral data are involved, they will be referred to as TBVIs).

2.4.1. Stepwise multiple-linear regression models

The stepwise maximum R improvement (MAXR) procedure in SAS 9.3 (SAS Institute Inc., 2011) was used to compute the Stepwise multiple-linear regression models (SMRMs). The MAXR procedure determines, iteratively, the combination of bands that give the best 1-band model, 2-band model, 3-band model…and so on to best n-band model of crop biomass and yield for each crop type. This procedure produces the best multiple linear regression parameter estimates (highest R^2 values) by looking at the incremental explanatory power of each variable in the regression data set, with equation in the form:

$$SMRM_i = \Sigma_{j=1}^{n} a_{ij} R_j \quad (1)$$

where i = crop variable, a = coefficient for reflectance in waveband j (j = 1 to n) for ith variable, and R = reflectance in wavebands j. This procedure was applied to both HNBs (n = 158) and MBBs (n = 4 to 9 depending on the sensor type — see Table 1) reflectance data.

2.4.2. Two-band vegetation indices

Linear and non-linear (logarithmic and exponential) correlation analyses between biomass or yield quantities and Two-Band Vegetation Indices (HVIs and TBVIs, Eq. (2)) of narrowband and broadband reflectance data were computed for each crop type using the correlation

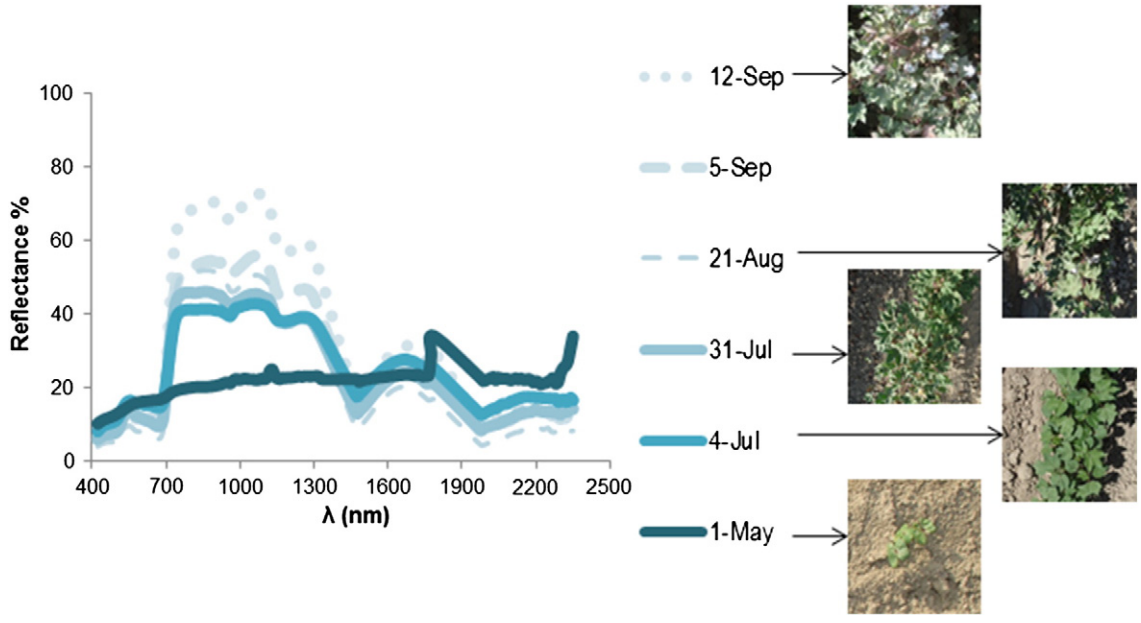

Fig. 2. Seasonal (May to September) vegetation spectra measured using ASD field spectroradiometer for a cotton field, and some photographs showing their respective biomass growth.

(CORR) procedure in SAS, taking every possible 2-band combinations of the input bands:

$$HVI_{ij} \text{ or } TBVI_{ij} = \frac{R_j - R_i}{R_j + R_i} \quad (2)$$

where i = band i, j = band j, and R = reflectance (%) of wavebands.

For Hyperion and spectroradiometer, a matrix of 158 × 158 = 24,964 HNBs was obtained. Considering that the indices above and below the matrix diagonal are transpose of one another, only 12,403 unique indices [(24,964–158)/2] were used. Of such a large number of HVIs, the redundant indices and their related wavebands were established, and the most valuable indices and their specific application were determined. The broadband vegetation indices (TBVI; Rouse et al., 1973) of ALI, ETM+, IRS, IKONOS, and QuickBird were also computed. For the 7 bands of Landsat ETM+ there were only 21 ($7 \times 7 = 49 - 7 = 42/2 = 21$) unique TBVIs. The results of correlation between the R^2 values involving HVIs and TBVIs with biophysical variables (*e.g.*, biomass, yield) were plotted in Lambda (λ_1, or wavelength bands 1 to 158) *vs.* Lambda (λ_2, or wavelength bands 2 to 158) contour plots. Coefficients having a *p*-value <0.05 (95% confidence level) were evaluated and reported.

2.5. Crop type discrimination and optimal band determination using narrowband and broadband data

Availability of data in discrete narrowbands through hyperspectral data provides many opportunities to study crop characteristics and explore the potential of better separating and classifying crop types when compared with the limited opportunities provided by broadband data. The methods used to discriminate crop types are discussed below.

2.5.1. Least squares means approach for crop type discrimination

Least squares means (Bretscher, 1995) were analyzed for assessing differences in band reflectance between three-, four-, and five-crop types (wheat, cotton, maize, rice and alfalfa) by month using hyperspectral and multispectral sensors. Pairwise comparisons of means, for the above combinations, were produced using the generalized linear model (GLM) procedure with the LSMEANS method in SAS. The tests were conducted using data from different months to see in which months the crops are best separated from each other, and which HNBs or MBBs provided the best results. The tests of significance were conducted at the 95% confidence level.

2.5.2. Stepwise discriminant analysis approach for crop type discrimination

Stepwise discriminant analysis (STEPDISC procedure in SAS, SAS Institute Inc., 2011) is a powerful approach to select a subset of the wavebands that best separate crop types. There are 2 distinct discriminant methods: (a) Wilk's lambda (Wilks, 1935) and (b) Pillai Trace (Pillai, 1955). The Wilk's lambda is the likelihood ratio criterion (ratio of within-group variance to the total variance) with a value ranging from 0 to 1. The higher the Wilk's lambda, the lesser the separability between crop types (0 means 100% separability of wheat, cotton, maize, rice, and alfalfa). When applied to the 158 bands of Hyperion, for example, this analysis begins with no waveband variables in the model. At each step, if the band that contributes least among the 158 bands to the discriminatory power of the model, as measured by the Wilk's lambda, fails to meet the criterion to stay, then that band is removed. Otherwise, the band not in the model that contributes most to the discriminatory power of the model is entered. When all bands in the model meet the criterion to stay and none others meet the criterion to enter, the process stops. Since many significance tests are performed, and the overall probability of rejecting at least one true null hypothesis is much larger than the significance level of each step, a very small significance level, $\alpha = 0.999$, was used. This was to avoid including any band that did not contribute to the discriminatory power of the model (SAS Institute Inc., 2011).

Finally, the Wilk's lambda values are plotted against the number of bands to determine the number of bands sufficient to best separate the 5 crops (when the curve becomes asymptotic or near-asymptotic) and their wavelength centers. A similar approach is used for Wilk's lambda tests with any other broadband or narrowband sensor.

2.5.3. Principal component analysis approach for crop type discrimination

Principal component analysis (PCA) (Pearson, 1901) establishes prominent bands most important for capturing highest variance in data, and helps eliminate data redundancy by identifying and eliminating less important bands. The PCA is explored for each crop (wheat, cotton, maize, rice and alfalfa) separately to determine how best the characteristics of that crop are captured. The PCA was performed using the PRINCOMP procedure in SAS. The resulting eigenvalues explain the variability in data explained by various PCAs, and the resulting eigenvectors associated with each band help determine the importance of the band (the higher the eigenvector, the greater the importance of the band). PCAs are applied to both HNBs and MBBs.

2.5.4. Correlation between narrowbands for determining optimal hyperspectral narrowbands

It is well known that the overwhelming proportion of HNBs and their derived HVIs are redundant for any given application. In this study, an extensive research on the redundant and useful Hyperion and spectroradiometer HNBs was conducted. The correlation between all possible combinations of narrowbands resulted in a total of 12,403 Pearson coefficients. The squared coefficients, R^2, values were plotted in Lambda (λ_1) by Lambda (λ_2) plots to determine the HNB-centers and widths that provide the best and the redundant information.

2.5.5. Discriminant model and error matrices for determining optimal hyperspectral narrowbands

To assess the sensors' accuracy in discriminating crop types, a linear discriminant function based on the pooled covariance matrix was performed using the discriminant analysis (PROC DISCRIM is SAS). The hyperspectral and multispectral band reflectivity data of the 5 crop types are fed into the discriminant model. The input wavebands were the most frequently occurring wavebands resulting from the LS-means, Wilk's lambda, PCA, and lambda–lambda plots of hyperspectral and multispectral data as discussed in previous sections. This results in error matrices (Congalton & Green, 2009). Omission errors were calculated as the ratio of false negatives to the total number of pixels belonging to a particular crop type. Commission errors were calculated as the ratio of the false positives to the total number of pixels belonging to a particular crop type. The overall classification accuracy is calculated as:

$$\text{Overall accuracy} = \frac{\sum_{i=1}^{k} n_{ii}}{n} \times 100(\%) \quad (3)$$

where n is the total number of validation pixels, n_{ii} is the number of pixels classified into crop type i (or diagonal agreement of the confusion matrix), and k is the number of crop types.

3. Results

First, the results of the crop biophysical modeling of biomass and yield of the 5 crops will be discussed using Hyperion and spectroradiometer HNBs and HVIs and compared with MBBs and TBVIs data from 5 multispectral sensors: Landsat ETM+, Advanced Land Imager (ALI), Indian Remote Sensing Satellite (IRS), IKONOS, and QuickBird. Second, the results of the ability of HNBs and MBBs in discriminating the 5 crops will be presented and discussed. In both crop productivity modeling and crop type discrimination, the results are obtained from multiple methods. This provides robustness to the results obtained.

Table 2
Hyperspectral narrowband and multispectral broadband stepwise multiple-linear regression models of wet biomass and yield. Note: blank areas indicate either absence of data or low sample size (n < 7).

		Spectroradiometer			Hyperion			ETM+		
Crop type	Biophysical variable	Sample size (n)	Best bands (λ = nm)	Best R^2	Sample size (n)	Best bands (λ = nm)	Best R^2	Sample size (n)	Best bands (λ = nm)	Best R^2
Cotton	Wet biomass	150	1084, 1104, 1548, 1689	0.65	16	933, 2052, 2285	0.95	38	483, 830, 1650	0.55
	Yield (cotton)	7	2153, 2184, 2194	0.98	15	752, 1477, 1770, 1790, 2063	0.99			
	Yield (cotton + add)	10	895, 1104, 2123, 2184	0.99	15	437, 2123, 2224, 2254	0.99			
Maize	Wet biomass	27	1054, 1215, 1558, 1841	0.96	9	427, 437, 973, 1165	0.99	14	483, 1650, 2220	0.62
Wheat	Wet biomass	24	1013, 1033, 1054, 1074, 1114, 1371	0.96				11	830, 2220	0.79
	Yield (wet)	11	518, 1144, 1155, 1477, 2032	0.97	23	864, 902, 1023, 1104, 1437, 1609, 1730	0.94			
	Yield (dry)	14	1982, 2174, 2184, 2194, 2285, 2335	0.93	23	590, 630, 640, 953, 1528, 1599, 1982, 2305	0.98			
Rice	Wet biomass	9	1013, 1720, 1730	1						
Alfalfa	Wet biomass	9	813, 953, 1134, 1371, 1821	0.99						

Third, the outcome of the synthesis of the results will lead to determining optimal wavebands (band centers and widths) and indices that best characterize, model, and discriminate irrigated crops.

3.1. Crop productivity modeling

3.1.1. Crop productivity models using hyperspectral narrowbands vs. multispectral broadbands

The results of the stepwise multiple-linear regression models (SMRMs) are presented in Table 2. The Hyperion and ASD spectroradiometer based SMRMs gave higher coefficients of determination (R^2) than multispectral sensors in all cases (9 out 9), with $0.94 < R^2 < 0.99$ for Hyperion, and $0.65 < R^2 < 0.99$ for spectroradiometer. Typically, when 3 to 8 HNBs, whether from Hyperion or spectroradiometer, are involved the R^2-values reach 0.93 to 1.0, except for cotton biomass with R^2-value = 0.65 for the spectroradiometer. The combination of narrowbands was mostly located in the SWIR (1300–2500 nm) and NIR, or SWIR and visible (400–700 nm) portions of the spectrum. More specifically, 53.6% of these narrowbands are represented by early mid-infrared (EMIR, 1301–1990 nm) and far mid-infrared (FMIR, 1901–2350 nm) with the most frequently occurring bands centered at 1371, 1731, 2121, 2181, and 2191 nm.

The spectroradiometer data also showed a high frequency in the far near-infrared (FNIR, 1051–1300 nm), with 1054 and 1104 being the most frequent bands. Lower coefficients of determination were obtained by the broadband sensors, particularly by ALI and the hyperspatial IKONOS and QuickBird, with R^2 ranging from 0.09 to a maximum of 0.56. Among the broadband sensors, ETM+ and IRS provided better results ($0.55 < R^2 < 0.79$, and $0.36 < R^2 < 0.73$, respectively). Overall, these R^2-values from the HNBs were higher by 0.09 to 0.35 (most frequently ≥0.25) when compared with MBBs. The overwhelming proportion of the HNBs is in the shortwave infrared region (SWIR) region followed by far infrared. In most cases about 4 HNBs were enough to obtain maximum R^2-values, often reaching 0.9. Of the MBBs, IRS, ALI, and ETM+ performed about the same, significantly better than IKONOS and QuickBird, but significantly poorer than HNBs of Hyperion and spectroradiometer. This also indicates that the very high spatial resolution (2–3 m) of IKONOS and QuickBird is not sufficient without the high spectral resolution available from sensors such as Hyperion.

3.1.2. Crop productivity models using two-band vegetation indices

A Lambda (λ_1) by Lambda (λ_2) correlation matrix between all possible combinations of two-band vegetation indices (TBVIs and HVIs) and biomass (wet and dry) and yield was obtained using HNBs and MBBs (Fig. 3a,b,c and Table 3). The best linear and non-linear models (logarithmic or exponential) are reported in Table 3. HVIs showed higher correlation with cotton and maize biomass and yield (R^2 = 0.92–0.96, and R^2 = 0.80–0.97, respectively; $p < 0.5$) when compared with TBVIs (maximum obtained R^2 was 0.79 for the ETM+ wheat biomass model). HVIs were mostly a combination of NIR and/or SWIR bands. Specifically, the most frequent bands were located in the FNIR (at 1245, 1276, and 1296 nm) and EMIR (at 1498, 1508, 1689, and 1699 nm) followed by FMIR (at 2194, 2285, and 2305 nm). Differences between the best narrowband and best broadband R^2 are reported. Wheat biomass and yield were best correlated to spectroradiometer HVIs than Hyperion HVIs and IRS, ALI, and IKONOS TBVIs. Rice biomass was also better detected by spectroradiometer HVIs compared to ETM+, IRS, and QuickBird TBVIs. One case of higher correlation of IRS TBVIs with alfalfa biomass (R^2 = 0.83) than spectroradiometer (R^2 = 0.64) is reported. Overall, hyperspectral HVIs outperformed multispectral TBVIs in 8 out 9 cases (see difference between best narrowband and best broadband R^2 in Table 3).

The Lambda (λ_1) by Lambda (λ_2) R^2-contour plots (Fig. 3a,b,c) represents the correlation between HVIs and biomass or yield. Of the R^2 matrix, only values above or below diagonal (12,403) are retained because they are transpose of one another. The areas of "bulls-eye" represent areas of maximum information content, where the best band centers and widths are determined. For example, R^2 values of 0.96 and 0.94 were achieved by Hyperion HVI697-1221 (HNBs centered at 697 nm and 1221 nm) and HVI1201-1171 (HNBs centered at 1201 nm and 1171 nm) respectively.

Overall, stepwise multiple-linear regression models (SMRMs) and the two band vegetation indices provided significantly better results than broadband data because of higher sensitivity at specific hyperspectral narrowband locations to plant pigmentation, canopy structure, and growing conditions (Thenkabail et al., 2011, 2002). In particular, 74% HNBs were located in the 1051–2331 nm range of the spectrum, including FNIR (1100–1300 nm), ~10% were located in the moisture sensitive near-infrared (MSNIR, 951–1050 nm), 6% in the red and red-edge (630–752 nm), and the remaining 10% distributed between blue (400–500 nm), green (501–600 nm), and NIR (760–900 nm).

3.2. Crop type discrimination using hyperspectral versus multispectral data

3.2.1. Differences in mean HNBs and MBBs spectra among crop types

Significant ($p < 0.05$) pairwise comparisons of all possible combinations of mean reflectance of three crops (cotton, maize, and wheat; or cotton, maize, and alfalfa), four crops (cotton, maize, wheat, and rice), and five crops (cotton, maize, wheat, rice, and alfalfa) for the months of June, July, and August using HNBs *versus* MBBs are reported in Table 4. Spectroradiometer data could significantly discriminate three (cotton, maize, and wheat) crop types in June and July, and four crop types (cotton, maize, wheat, and rice) in July, when they are in full growth stage, with bands mostly located in the EMIR (1330–1900 nm) and FMIR (1901–2350 nm), followed by the red portion (600–700 nm) of the spectrum. However, it performed poorly in discriminating alfalfa from other crop types. From the second half of June until the end of July, the leaf senescence of the alfalfa crops as well as the high

ALI			IRS			IKONOS			QuickBird		
Sample size (n)	Best bands (λ = nm)	Best R^2	Sample size (n)	Best bands (λ = nm)	Best R^2	Sample size (n)	Best bands (λ = nm)	Best R^2	Sample size (n)	Best bands (λ = nm)	Best R^2
			160	555, 815	0.56	24	490, 565, 805	0.56	12	485, 560, 660	0.09
25	565, 660	0.16	17	555, 815	0.59	34	680, 805	0.14			
25	482.5, 565, 660	0.2	17	555, 815	0.64	34	680	0.1			
			18	555, 650, 1625	0.73						
			16	650, 1625	0.36						
7	443, 482.5, 565, 660	0.63	10	650	0.68	10	490, 680, 805	0.28			
7	443, 482.5, 565, 660	0.71	10	650	0.73	10	490, 680, 805	0.35			
			15	555, 650, 815	0.66						

soil background effect could have affected the reflectance, and made the spectral discrimination of alfalfa from other crops more complex. Only the bands centered at 2441 and 2551 nm were significantly able to discriminate all the five crop types. Indeed, bands in the very far mid-infrared of the spectrum are particularly sensitive to soil background effect and plant stress (Thenkabail, Enclona, Ashton, & Van Der Meer,

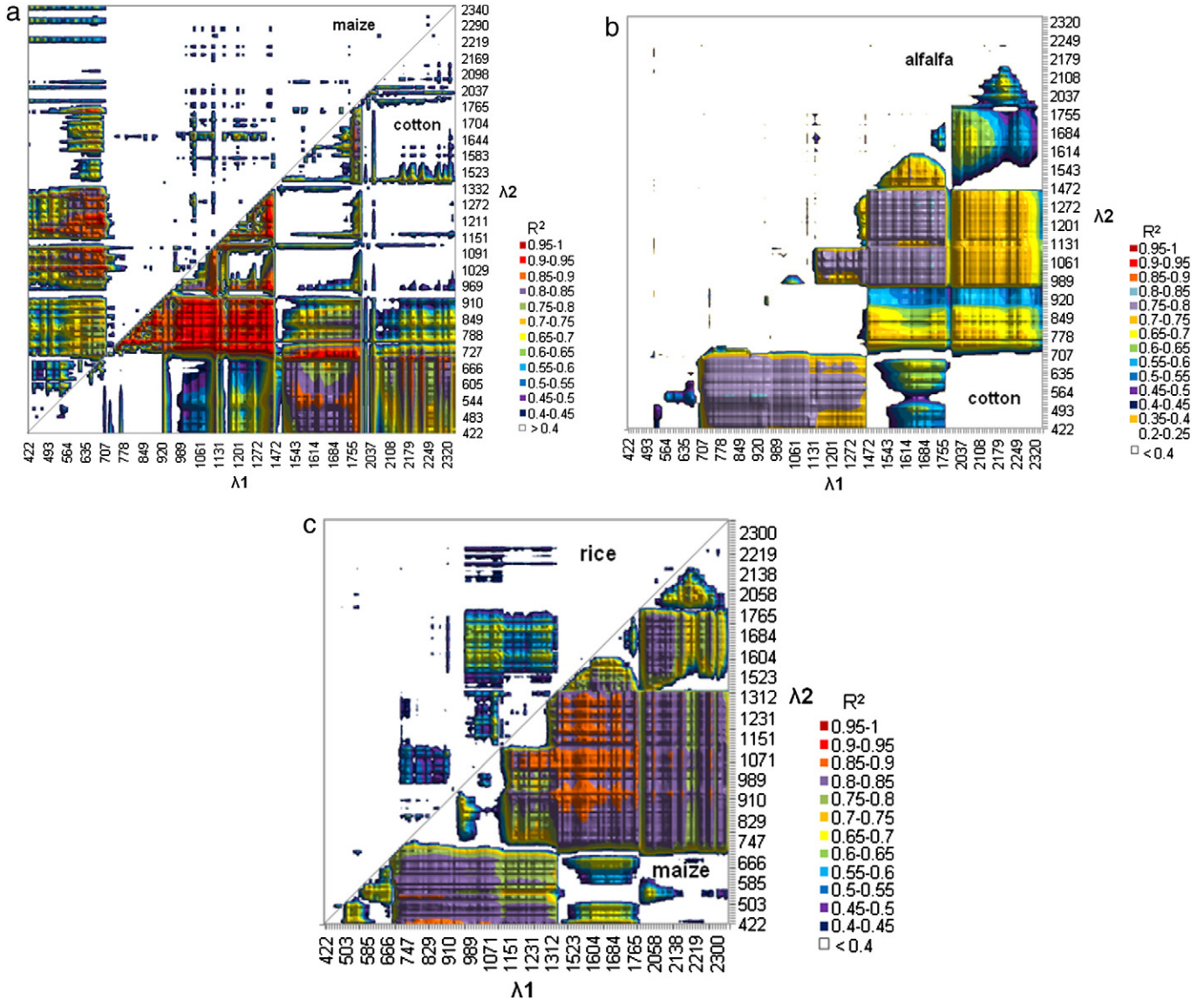

Fig. 3. Crop biomass models using hyperspectral vegetation indices. λ_1–λ_2 non-linear logarithmic R^2 correlation values of: (a) Hyperion HVIs *vs.* wet biomass of cotton (below diagonal) and maize (above diagonal); (b) Spectroradiometer HVIs *vs.* wet biomass of cotton (below) and alfalfa (above); (c) Spectroradiometer HVIs *vs.* wet biomass of maize (below) and rice (above).

Table 3
Linear and non-linear relationships between two-band vegetation indices and biomass and yield. Note: blank areas indicate either absence of data or low sample size (n < 7).

	Spectroradiometer						Hyperion						ALI					
	n	Model	λ1	λ2	R^2	*p*	n	Model	λ1	λ2	R^2	*p*	n	Model	λ1	λ2	R^2	*p*
Cotton																		
Wet biomass	165	Linear	2194	2083	0.50		33	Linear	2194	1528	0.63		8	Linear	7	2	0.64	
		Non-linear log	1720	1306	0.80			Non-linear log	742	1175	0.94			Non-linear exp	3	2	0.58	
Dry biomass							33	Non-linear log	834	824	0.91							
Yield cotton	7	Linear	1699	1689	0.95		15	Linear	1296	1054	0.92	25	$p > 0.05$					
		Non-linear exp	1699	1689	0.97			Non-linear exp	1296	1054	0.92							
Yield cotton add	10	Linear	1023	1003	0.86		15	Linear	1205	1044	0.93		25	$p > 0.05$				
		Non-linear log	1316	1286	0.89			Non-linear exp	1296	1044	0.92							
Maize																		
Wet biomass	28	Linear	518	427	0.77		9	Linear	1033	722	0.92		9	$p > 0.05$				
		Non-linear log	1276	1094	0.91			Non-linear log	1225	697	0.96							
Dry biomass							9	Non-linear log	1104	702	0.96							
Wheat																		
Wet biomass	83	Linear	1235	1114	0.45		30	Linear	1155	1013	0.25			$p > 0.05$				
		Non-linear log	2042	712	0.44			Non-linear log	2153	2093	0.25							
Dry biomass								Non-linear exp	1750	1689	0.25							
Yield wet	11	Linear	2285	1498	0.74		23	Linear	1276	1245	0.41		7	$p > 0.05$				
		Non-linear exp	2285	1498	0.75			Non-linear log	2305	1508	0.45							
Yield dry	14	Linear	2093	1508	0.63		23	Linear	1276	1245	0.40		7	$p > 0.05$				
		Non-linear exp	2103	1508	0.64			Linear	2305	1508	0.40							
								Non-linear log	2305	1508	0.43							
Alfalfa								–						–				
Wet biomass	18	Linear	1740	1609	0.57													
		Non-linear exp	488	447	0.64													
Rice								–						–				
Wet biomass	14	Linear	1165	1023	0.67													
		Non-linear log	1215	1094	0.75													

2004). Yet, the classification of alfalfa pixels reflectance across the total growing season was 100% accurate using spectroradiometer data (see Table 7).

Numerous Hyperion bands significantly discriminated among cotton, maize, and wheat in August. These three crop types were also distinguished by some multispectral sensors: in the month of June by ALI but not by ETM+; in July by IRS, ETM+, and the hyperspatial IKONOS and QuickBird; and in August by ETM+. In June and July, the four and five crop types were distinguished by IRS, but not by QuickBird.

Overall, the high number of HNBs of Hyperion and spectroradiometer provides far greater opportunities than MBBs in differentiating a greater number of crops. Indeed, vegetation has a very distinctive spectral signature dependent on its different concentration of water molecules (peak in the NIR), pigments such as chlorophyll (VIS, NIR), carotenoids (UV), and anthocyanins, and cell wall structural polysaccharides, such as cellulose and lignin (SWIR) (Gitelson, 2011; Thenkabail, Lyon and Huete, 2011). Hence, the greater number of narrow bands is useful in detecting and modeling these specific features. Furthermore, when crops are difficult to differentiate in MBBs, one can find one HNB or the other (or a combination of HNBs) that can help differentiate crop types. This is especially useful when remote sensing data are available only in few months.

3.2.2. Stepwise discriminant analysis of crop types

The ability of HNB and MBB data to discriminate crop types was examined using the stepwise discriminant analysis. The degree of separability (at $p < 0.0001$; 99% confidence level) among cotton, maize, and wheat using HNB data from Hyperion and spectroradiometer, and MBB data from ALI, ETM+, and IKONOS is shown in Fig. 4. It must be noted that lower Wilk's λ represents greater separability between crops. A high degree of near perfect (~100%) discrimination (Wilk's $\lambda \approx 0$) between cotton, maize, and wheat crops was achieved by Hyperion using 54 wavebands (Fig. 4a). Of these 54 bands, 48% were in the NIR, 33% in the SWIR, and 19% in the VIS portion of the spectrum. The same level of separability using spectroradiometer (Wilk's $\lambda \approx 0$) was achieved using 14 wavebands, 79% of which in the VIS and 21% in the NIR. Relative to the HNBs, the MBBs performed much poorer in separating crop types: ETM+ reaches a Wilk's λ of 0.6094 with 4 non-thermal bands; IKONOS a Wilk's λ of 0.5644 with 4 bands; and ALI a Wilk's λ of 0.2728 with 7 bands. Still, the spectroradiometer performed better (Wilk's $\lambda = 0.00144$) than ETM+ (Wilk's $\lambda = 0.5594$) in discriminating cotton, maize, and rice using six bands only, 67% of which in the VIS and 33% in the NIR, *versus* three ETM+ bands (Fig. 4b). This shows substantial inter-mix among crop types.

3.2.3. Principal component analysis of hyperspectral narrowband data

The purpose of the principal component analysis (PCA) was to reduce the redundancy of the hyperspectral wavebands by computing a minimum set of unique bands (up to 5) that best explain the variability in reflectance. Table 5 displays the PCAs of Hyperion and spectroradiometer narrowbands across the different crop types. For Hyperion, the first PCA explains 66% of the total variance in cotton fields, the second PCA explains 24%, up to the fifth explaining 1%. Two to five PCAs provide an accurate summary of the data, with two PCAs accounting for 90% of the total variance and five explaining 98%. The most important Hyperion HNBs involved with cotton PCA1 were 1608 nm, 1588 nm, 1568 nm, 1578 nm, and 1598 nm (Table 5). Overall, for cotton, PCA1 was determined by HNBs in the EMIR (1300–1900 nm) and the PCA2 by the NIR (760–900 nm) wavebands. For maize crops, the first two and first five PCAs explained 79% and 93% of variance, respectively, with the first PCA determined mostly by EMIR, and PCA2 by FMIR wavebands. For wheat crops, the first two and first five PCAs explained 93% and 98% of variance respectively. PCA1 was determined by EMIR and PCA2 by FNIR. For spectroradiometer, the first two and the first five cumulative principal components explained respectively 93% and 99% of variability of alfalfa field reflectance, 88 and 99% of cotton fields, 94 and 99% of maize fields, 97 and 100% of rice fields, and 93 and 100% of wheat fields. As in Hyperion, the wavebands dominating in spectroradiometer PCA1s were located in the EMIR, and in PCA2s in the NIR for the five crops. Overall, across the crops, for Hyperion or spectroradiometer, the first 2 PCAs explained about 90% variability and were dominated by HNBs in EMIR (1300–1900 nm) and NIR (760–900 nm) with sprinkling of bands from other wavelengths.

ETM+						IRS						IKONOS						QB		Difference between best narrowband R2 and best broadband R2
n	Model	λ1	λ2	R^2	p	n	Model	λ1	λ2	R^2	p	n	Model	λ1	λ2	R^2	p	n		
53	Linear	3	1	0.38		160	Linear	3	2	0.56		25	Linear	4	3	0.45		12	$p > 0.05$	0.26
	Non-linear log	3	1	0.65			Non-linear log	3	2	0.68			Non-linear log	4	3	0.63				
						18	Linear	3	2	0.57		34	Non-linear exp	4	3	0.18			–	0.31
							Non-linear log	3	2	0.66										
						23	Linear	3	2	0.59		34	Non-linear exp	4	3	0.18			–	0.22
							Non-linear log	3	2	0.71										
14	Linear	3	2	0.45		18	Linear	2	1	0.62		9	$p > 0.05$					3	$p > 0.05$	0.09
	Non-linear log	3	2	0.59			Non-linear log	3	2	0.87										
						16	Linear	4	3	0.36			–						–	0.03
							Non-linear exp	4	3	0.42										
	–					10	Linear	3	2	0.62		10	$p > 0.05$						–	0.13
							Non-linear log	3	2	0.57										
	–					10	Linear	2	1	0.56		10	$p > 0.05$						–	0.01
							Non-linear log	3	2	0.63										
	–												–						–	
						15	Linear	2	1	0.70										−0.19
							Non-linear log	3	2	0.83										
14	Linear	4	1	0.29			$p > 0.05$											5	$p > 0.05$	0.42
	Non-linear log	5	4	0.33																

3.2.4. Correlation between hyperspectral narrowbands data

The correlation analysis between the 158 narrowbands of Hyperion and spectroradiometer resulted in 12,403 R^2 values each. The λ_1–λ_2 contour plots of cotton and wheat for Hyperion and spectroradiometer are shown in Figs. 5 and 6. The areas of high correlation (high R^2 values, blank regions) between two wavebands signify band redundancy; thus, areas of lowest R^2 are the most informative. For wheat, the most informative bands of both Hyperion and spectroradiometer are located in the NIR and the visual portion of the spectrum followed by FMIR and EMIR. For cotton, the most common Hyperion bands are located across the entire spectrum, mostly in the red-edge and FNIR, and the most common spectroradiometer bands are located in the blue, red-to-FNIR, and FMIR.

3.2.5. Frequency of occurrence of HNBs and MBBs, accuracies of crop type classification, and selection of best bands

Accuracy in discriminating crop types was examined by discriminant analysis using the most frequently occurring wavebands resulting

Table 4
Least square means of crop types reflectance showing significant statistical discrimination power at $p < 0.05$ (95% confidence level) for hyperspectral narrowbands and multispectral broadbands.

	Cotton Maize Wheat			Cotton Maize Alfalfa	Cotton Maize Wheat Rice		Cotton Maize Wheat Rice Alfalfa	
	Band centers (nm)			Band centers (nm)	Band centers (nm)		Band centers (nm)	
	June	July	August	August	June	July	June	July
Spectroradiometer	581, 591	610–681, 702, 1441–1451, 1588–1740, 1961–2073, 2133–2194, 2214		$p > 0.05$	$p > 0.05$	427–498, 610–681, 702 1441–1451, 1588–1740, 2081–2193, 2214, 2244–2285	$p > 0.05$	$p > 0.05$
Hyperion			437, 468–529, 569–712, 722, 752, 763, 875–925, 933–1336, 1477–1498, 1790, 2073, 2093, 2103, 2123–2153, 2174, 2244, 2264, 2285, 2305–2355					
ALI			565, 660, 790, 1250, 1650, 2215					
IRS	815, 1625	650, 815		555, 815	815, 1625	650, 815	815, 1625	650
ETM+	$p > 0.05$	565, 660, 825	825		$p > 0.05$	660, 825		
IKONOS		680, 805						
QuickBird		830				$p > 0.05$		$p > 0.05$

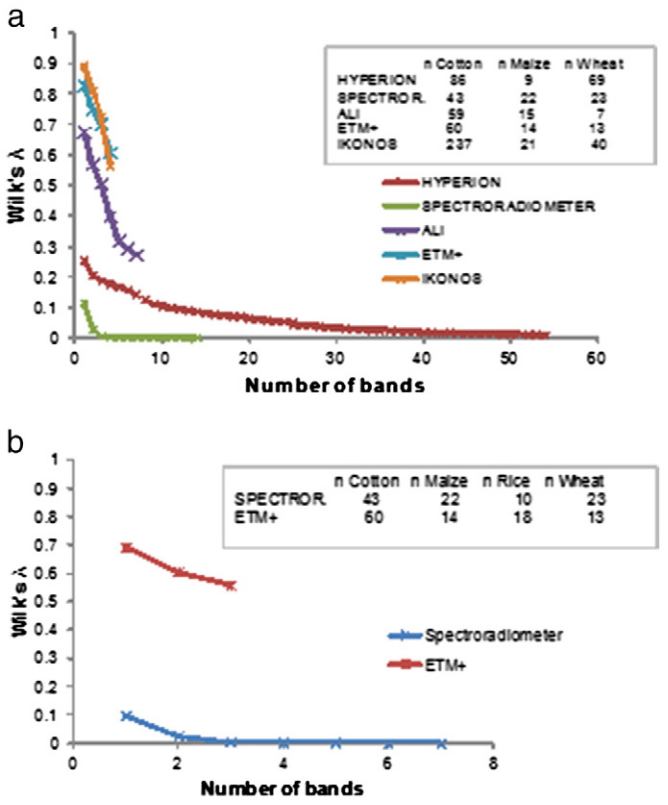

Fig. 4. Crop type discrimination (3 crops involved) using hyperspectral narrowbands: (a) Wilk's lambda separability of cotton, maize, and wheat for spectroradiometer, Hyperion, ALI, ETM+, and IKONOS. (b) Wilk's lambda separability of cotton, maize, and rice for spectroradiometer and ETM+. Note: Lesser the Wilk's Lambda, greater the separability. n = number of pixels examined.

from the LS-means, Wilk's lambda, PCA, and lambda–lambda correlation matrix for the hyperspectral sensors, and LS-means and Wilk's lambda for the multispectral sensors (Fig. 7).

The ranking of the best bands was used as input bands for classifying the crop types. When bands ranked within the same group (*e.g.* 680 nm and 690 nm) contained redundant information, only one band was selected as input. Such an approach helps in overcoming the Hughes' phenomenon (Thenkabail et al., 2011). Based on this approach, the best 3, 5, 9, 12, 15, and 29 Hyperion bands were selected (Table 6). An overall accuracy of 90.2% was achieved using 29 narrow bands in classifying cotton, corn, and wheat crops. It took 21 spectroradiometer bands to achieve a classification accuracy of 92% (Table 6). The results of the confusion matrix from the best 21 spectroradiometer wavebands are shown in Table 7. When comparing the crop types, the best accuracy classification was found for alfalfa and maize (100%), followed by cotton (97.7%), wheat (95.6%), and least rice (30%). The largest error occurred for rice pixels misclassified as wheat with an omission error of 70%, probably due to water background reflection. In contrast, the overall accuracy of MBBs in crop type discrimination is lower than narrowbands even when using all the bands and for two crops only (cotton and wheat), as in the case of IRS (overall accuracy = 92.6%) (Table 6). Comparing the accuracy in discriminating the same three crops – cotton, maize, and wheat – between the multispectral ALI and IKONOS and hyperspectral Hyperion, the latter outperformed with only 12 bands (overall accuracy = 86%). ALI and IKONOS reached a maximum accuracy of 83.9% and 76.8% respectively using 9 and 4 bands respectively. The overall accuracy of the 6 non-thermal ETM+ bands was 54.3% in discriminating four crop types (cotton, maize, wheat, and rice), poor compared to the spectroradiometer which, with only one band centered at 432 nm, could discriminate the same four crop types as well as a fifth crop, alfalfa, with 71.2% accuracy. However, it is important to note that it is possible to achieve over 90% classification accuracies using HNBs even when a greater number of crop types is involved, as illustrated for 5 crops using spectroradiometer data (Table 7). For MBBs the classification accuracies decrease swiftly with greater number of crop types.

4. Discussion and conclusions

This study examined the performance of hyperspectral narrowband data from Hyperion and spectroradiometer *versus* multispectral broadband data from ETM+, ALI, IRS, IKONOS, and QuickBird in assessing crop biomass and yield, and in discriminating five key world crops (cotton, wheat, maize, rice, and alfalfa). The best biophysical models were established based on: 1. stepwise multiple linear models involving hyperspectral narrowbands (HNBs) and multispectral broadbands (MBBs); and 2. linear and non-linear models resulting from two-band vegetation indices (TBVIs) derived from MBBs, and hyperspectral vegetation indices (HVIs) derived from HNBs.

The best HNB models explained variability in biophysical parameters overwhelmingly above 93%, which is ~25% higher than the best MBB models. When comparing Hyperion with Landsat ETM+ and ALI that have the same spatial resolution of 30 m in the VIS, NIR, and MIR bands, Hyperion single reflectance bands and VIs performed better in detecting crop biomass and discriminating crop types. Among the multispectral sensors, IRS provided the best results followed by ETM+. The lowest correlation coefficients were determined by the hyperspatial IKONOS and QuickBird. This was as a result of differences in spectral, temporal, and spatial resolution of the images (Table 1). First, the spectral resolution issue: IKONOS and Quickbird have only 4 spectral bands in the visible and NIR portions (450–900 nm) when compared to more spectral bands and/or spectral bands spread across visible, near infrared, and short-wave infrared (Table 1). Second, the temporal resolution issue: the number of images analyzed was only two in the case of IKONOS and one in the case of QuickBird; in comparison, there were 5 ETM+, 2 ALI (note it has 9 bands), and 13 IRS images. The better results from IRS could be specifically attributed to greater temporal coverage. Third, the spatial resolution issue: one naturally sees greater spatial variability with finer spatial resolutions from QuickBird and IKONOS, whereas with coarser resolution imagery, such as Landsat ETM+, there is greater "averaging" of variability that, many times, leads to greater correlations with biophysical quantities, especially in highly variable heterogeneous farms. Further, it must be noted that Hyperion and ASD spectroradiometer did not yield the exact same results even though they were analyzed at the same spectral resolution (10 nm). Indeed, they differed in the following 3 factors: 1. Time of acquisition (the Hyperion images were acquired within a few days of spectroradiometer measurements); 2. Number of acquisitions (3 Hyperion images in 2007 as opposed to spectroradiometer data acquired every 15 to 20 days during the entire growing seasons of 2006 and 2007); and 3. Spatial resolution (30 m for Hyperion and 0.1134 m for spectroradiometer). At different scales, variability in reflectances and VIs is different because at very fine scale soil, shade, and other effects are well detected, while at coarser spatial resolutions these elements become blended and aggregated. When comparing Hyperion with sensors – Landsat ETM+ and ALI – having the same spatial resolution of 30 m in the VIS, NIR, and MIR bands, Hyperion single reflectance bands and VIs performed better in detecting crop biomass and discriminating crop types. Therefore, detection of plants biophysical properties is lost at coarser spectral resolution. Future studies should take these factors into consideration for intercomparison of sensor results. While this study was not focused on the spatial scale issue, an open question for future studies would be to establish the scale necessary to detect crop productivity and type discrimination, which could be done, *e.g.*, by simply resampling the images pixel size. The future HyspIRI satellite is being designed with a lower spatial resolution – 60 m – than Hyperion in the short wave infrared (VSWIR: 380 nm–2500 nm), and equal spectral resolution of 10 nm contiguous bands (National Aeronautics & Space Administration, 2013). Therefore,

Table 5
The best hyperspectral narrowband centers for the first five PCAs, selected based on factor loadings (eigenvectors) across different crop types.

	% Variability explained													
	PCA1	PCA2	PCA3	PCA4	PCA5	PCA1	PCA2	PCA3	PCA4	PCA5	First two cumulative PCAs	First three cumulative PCAs	First four cumulative PCAs	First five cumulative PCAs
	b center (nm)	b center (nm)	b center (nm)	b center (nm)	b center (nm)									
Hyperion														
Cotton	1608	885	732	437	427	66	24	5	2	1	90	95	97	98
	1588	875	712	963	732									
	1568	824	722	1992	722									
	1578	854	742	953	742									
	1598	793	773	973	2042									
Maize	722	1982	1124	943	1144	69	11	5	4	4	79	85	89	93
	1558	1992	2335	933	1134									
	1608	1488	933	1488	1982									
	1638	2083	2204	2063	1992									
	1679	2153	2244	2163	2264									
Wheat	1568	1064	773	915	1134	66	27	2	0.9	0.6	93	96	97	98
	1578	1104	752	885	1124									
	1608	1084	763	895	1144									
	1619	1094	783	864	1155									
	1629	1054	793	875	963									
Spectroradiometer														
Alfalfa	1769	1023	539	1790	681	48	45	5	1	0.6	93	98	99	99
	2254	1003	549	2355	671									
	1528	993	529	2335	661									
	1518	1013	427	1780	691									
	2224	963	559	1477	2073									
Cotton	488	1669	640	447	2355	56	32	9	1	0.9	88	97	98	99
	498	1679	702	549	2042									
	478	1659	773	437	1982									
	508	1649	661	427	2052									
	559	1689	691	457	2073									
Maize	681	1750	2355	2355	2305	54	40	2	1	0.7	94	97	98	99
	671	1740	2345	2345	2335									
	2042	1730	2335	1790	2315									
	2032	1599	2325	2325	2224									
	2052	1609	2295	549	2274									
Rice	1528	915	712	722	712	57	40	2	0.6	0.4	97	99	99	100
	1518	905	722	732	702									
	1508	880	701	2325	590									
	1538	885	549	712	2325									
	1548	895	559	963	1074									
Wheat	722	875	427	2345	2345	76	18	5	0.8	0.2	93	99	99	100
	712	854	437	2355	2355									
	1720	864	447	2315	712									
	1709	834	457	2335	702									
	1679	824	468	2325	722									

comparison of HyspIRI with Hyperion HNB crop models could provide insights on the spatial scale issue.

Examination of reflectance spectra from Hyperion and spectroradiometer crop productivity models provided the opportunity to determine the most frequently occurring and then the most valuable HNBs in predicting biomass. Of these, 74% were located in the FNIR, EMIR, and FMIR (1051–2331 nm) spectral range; 10% in the moisture sensitive 970 nm (NIR); 10% in the 400–550 nm (blue), 501–600 nm (green), and 760–900 nm (NIR); and 6% in the red and red-edge (630–752 nm). Likewise, the best HVIs for crop biophysical modeling and crop type discrimination involved HNBs centered at: (i) 742 nm and 1175 nm (HVI742-1175), (ii) 1296 nm and 1054 nm (HVI1296-1054), (iii) 1225 nm and 697 nm (HVI1225-697), and (iv) 702 nm and 1104 nm (HVI702-1104). These best bands are overwhelmingly (70%) located in the far-NIR infrared (FNIR) (1051–1300 nm), and 30% in the red-edge (701–750 nm) or most absorption portion of red (670–700 nm). The role of NIR (751–1050 nm) and FNIR bands in detecting crop biophysical properties and crop productivity has received recent attention for its sensitivity to chlorophyll content in the plant. Indeed, NIR and FNIR follow photosynthesis much better than the absorption visible red portion of the spectrum (Ollinger, 2011). This is because the visible bands (narrow and broad) saturate at the 1st leaf layer it encounters (since 95% of signal is absorbed at this stage), yet there are more leaf layers below the canopy with leaves plenty of chlorophyll. Recently, Gitelson (2011) reported the ~2–4th leaf layer in a corn canopy as having the maximum chlorophyll content. The only remote sensing bands that can see the middle leaf layers of a canopy are in the NIR or FNIR (as these can supposedly penetrate through seven leaf layers). Therefore, the NIR can indirectly sense much information of value to crop biophysical and crop productivity modeling. In addition, both FNIR and early mid-infrared (1301–1900 nm) are known to be sensitive to biomass and LAI (Thenkabail, Enclona, Ashton, Legg et. al., 2004), while both early mid-infrared and especially far mid-infrared bands (1901–2500 nm) provide valuable information on lignin, cellulose, and starch content in the plant, as well as the geometric structure of canopies, optical properties of underlying soils (Boyd and Ripple, 1997, and Boyd et al., 1999), and in handling complex dissimilar growth stages and growing conditions (Thenkabail, et al., 2002; Thenkabail et al., 2000). The high proportion of wavebands in FNIR, early mid-infrared (EMIR), far mid-infrared (FMIR), and followed by far near-infrared (FNIR) found in this study indicates the importance of using these waveband regions in establishing crop characteristics,

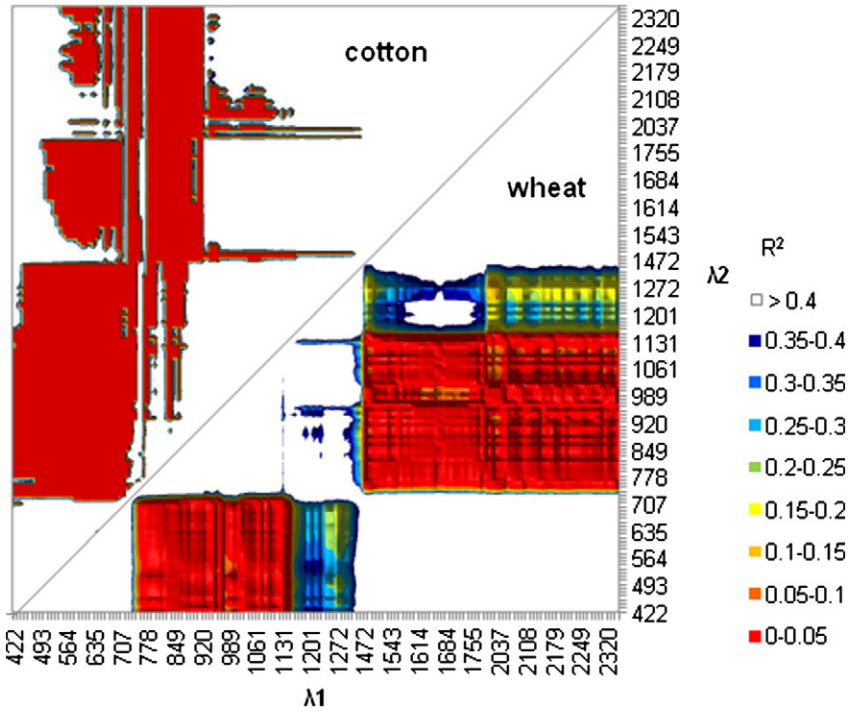

Fig. 5. Data redundancy and mining of hyperspectral narrowbands. Hyperion R^2 correlation values between λ_1 and λ_2 for cotton (above diagonal) and wheat crops (below diagonal). Note: Lesser the R^2 values, greater the uniqueness between two bands. Greater the R^2 values, greater the redundancy.

which are often ignored by traditional red and NIR based broadband NDVIs. This finding confirms similar results reported in previous studies of Kalacska and Sanchez-Azofeifa (2008), Thenkabail, Enclona, Ashton, Legg, et al. (2004), and Thenkabail, Enclona, Ashton and Van Der Meer (2004) who established MIR and FNIR as the most informative band regions in characterizing certain crop or other vegetation parameters.

Examination of reflectance spectra of the different crop types indicates that hyperspectral data provide many possibilities for discriminating different crops using either specific single bands mostly located in the mid-infrared and some in the red-edge or red, or a combination of bands in the entire spectrum but typically in the NIR and MIR. These bands, again, are useful to detect plant biochemical properties, biomass, and vegetation growth, which vary among plant species. Indeed, the overall accuracies of crop type discrimination were above 90% when ~20 HNBs were used, significantly higher than any of the broadbands which provided an accuracy varying between 45 and 84%. The best Hyperion HNBs that achieved greatest accuracies in crop type

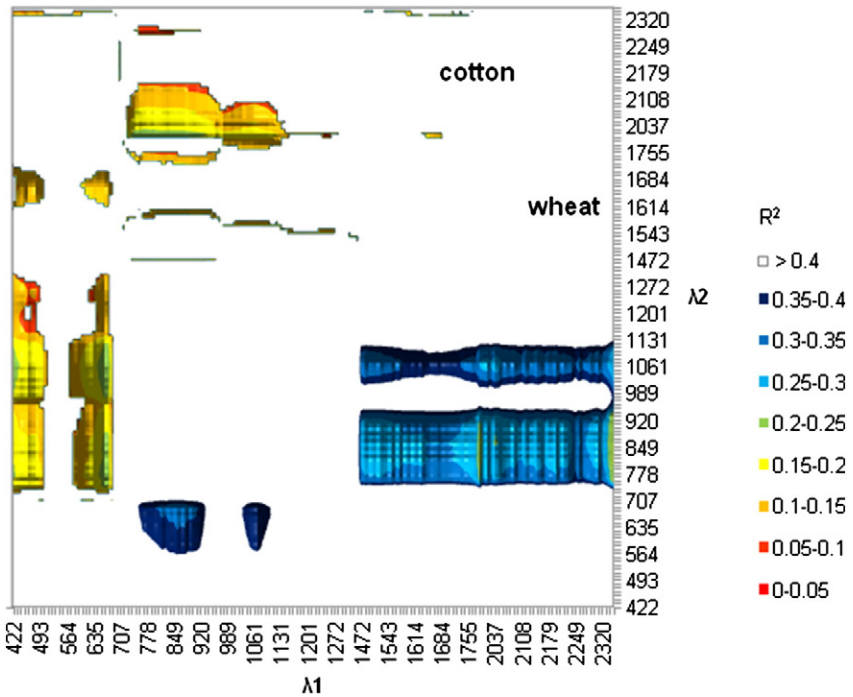

Fig. 6. Data redundancy and mining of hyperspectral narrowbands. Spectroradiometer R^2 correlation values between λ_1 and λ_2 for cotton (above diagonal) and wheat crops (below diagonal). Note: Lesser the R^2 values, greater the uniqueness between two bands. Greater the R^2 values, greater the redundancy.

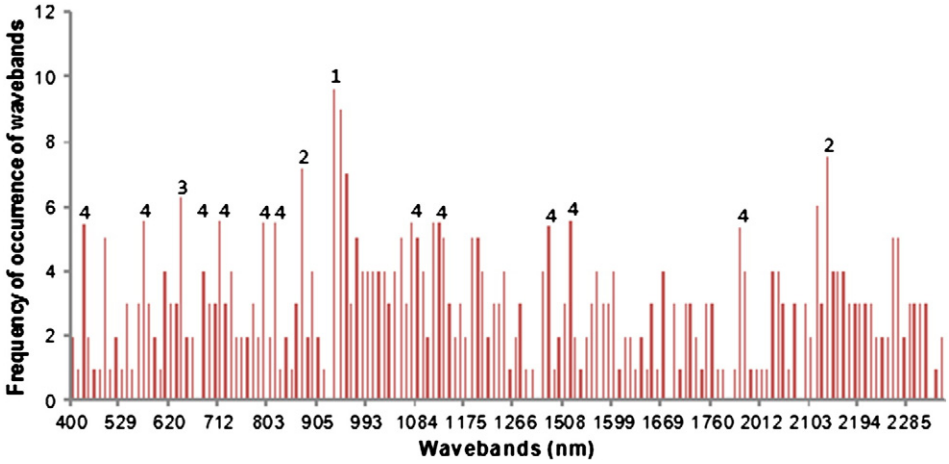

Fig. 7. Frequency of occurrence of Hyperion narrowbands in LS-means, Wilk's lambda, PCA, and λ_1–λ_2 R^2. Groups of close narrowbands most frequently occurring (frequency ≥6) are ranked by progressive numbers above columns (1 = most frequent).

discrimination are listed in Table 6. These accuracies range from 81.1% for 3 HNBs to 90.2% for 29 HNBs. The 29 HNB waveband centers of Hyperion were: 447, 508, 579, 651, 681, 722, 803, 824, 885, 933, 943, 953, 963, 983, 1064, 1084, 1094, 1124, 1134, 1144, 1195, 1205, 1488, 1528, 1982, 2123, 2143, 2264, and 2274. The accuracy of the spectroradiometer in discriminating five crop types was as well high ranging from 92% using 21 bands to 93.7 using 80 bands (Table 6). We do recommend the use of 21 bands over the 80 bands, as only 2% more information is gained with 59 more bands. This implies that a large number of HNBs are, typically, redundant in classifying crop types or modeling crop biophysical or biochemical quantities. Of the above mentioned spectroradiometer 21 bands that discriminated cotton, maize, wheat, rice, and alfalfa, three bands were in common with the Hyperion bands that discriminated cotton, maize, and wheat: band 681, 1124, and 1982. The waveband 681 (red) is a region of high light absorption of chlorophyll in green vegetation, and was reported (more specifically the band centered at 680 nm) by Thenkabail et al. (2000) as the most commonly occurring and most critical band canter for crop discrimination. It was also reported by Galvão et al. (2009) as a fundamental Hyperion band to discriminate soybean varieties, and by Clevers et al. (2007) in predicting grass biomass. The waveband 1124 (FNIR) corresponds to the reflectance postpeak 1 in 1050–1300 nm, which is particularly sensitive to biomass and LAI, and was reported by Thenkabail, Enclona, Ashton, Legg, et al. (2004) and Thenkabail, Enclona, Ashton and Van Der Meer (2004) as one of the informative Hyperion bands in explaining vegetation variability, and by Galvão et al. (2009), again, as

Table 6
Overall accuracies, determined by discriminant model, of best and all multispectral broadbands, and best hyperspectral narrowbands in discriminating 2 to 5 crop types.

	Crop types	No. of bands and spectrum	Band centers	Overall accuracy (%)
ETM+	Cotton, Maize, Rice, Wheat	2: green, NIR	565, 825	45.7
		All		54.3
IRS	Cotton, Wheat	2: red, SWIR	650, 1625	88.2
		All		92.6
ALI	Cotton, Maize, Wheat	2: red, NIR		59.2
		All		83.9
IKONOS	Cotton, Maize, Wheat	2: green, NIR	660, 1250	49.7
		All		76.8
Hyperion	Cotton, Maize, Wheat	3: NIR, FMIR	885,943,2143	81.1
		5: blue, red, NIR, FMIR	447,651,885,943,21443	82.3
		9: VIS, Red edge, NIR, MIR	447,579,651,681,722,803,885,943,2143	83.5
		12: VIS, Red edge, NIR, FNIR, EMIR, FMIR	447,579,651,681,722,803,885,943,1084,1134,1488,2143	86
		15: VIS, Red edge, NIR, FNIR, EMIR, FMIR	447,579,651,681,722,803,885,943,1084,1134,1488,1528,1982,2123,2143	87.2
		29: VIS, Red edge, NIR, MSNIR, FNIR, EMIR, FMIR	447,508,579,651,681,722,803,885,933,943,953,963,983,1064,1084,1094, 1124,1134,1144,1195,1205,1488,1528,1982,2123,2143,2264,2274	90.2
Spectr.	Cotton, Maize, Wheat, Rice, Alfalfa	1: blue	437	71.2
		2: blue, red	437, 681	75.7
		4: blue, red, NIR, FMIR	437, 681, 773, 1992	77.5
		7: blue, red, NIR, FNIR, FMIR	437, 681, 773, 1074, 1992, 2143, 2335	83.8
		11: blue, red, NIR, FNIR, EMIR, FMIR	437,681,773,1074,1124,1477,1609,1740,1992, 2143,2335	84.7
		21: blue, red, NIR, FNIR, EMIR, FMIR	437,457,478,498,620,640,651,671,681,773,1074,1124,1477,1609,1740, 1982,1992,2143,2335	93.7
		80: VIS, NIR, MSNIR, FNIR, EMIR, FMIR	427,437,447,457,468,478,488,498,508,590,600,610,620,630,640,651,661, 671,681,691,712,732,742,763,773,783,793,803,813,824,834,844,854,864, 875,885,895,905,915,925,953,963,973,983,993,1003,1013,1033,1044,1054, 1064,1084,1094,1104,1114,1124,1134,1144,1477,1599,1609,1659,1669, 1679,1740,1750,1790,1982,1992,2032,2042,2052,2063,2073,2083,2103, 2113,2123,2133,2335	92

Table 7
Classification accuracy matrix of 5 crops using best 21 spectroradiometer narrowbands (blue, red, NIR, FNIR, EMIR, FMIR).

	Observed crop types	Classified crop types					Omission error %	Commission error %
		Alfalfa	Cotton	Maize	Rice	Wheat		
No. observations classified into crop type	Alfalfa	13	0	0	0	0	0	0
% Classified into crop type		100	0	0	0	0		
No. observations classified into crop type	Cotton	0	42	1	0	0	2.3	0
% Classified into crop type		0	97.67	2.33	0	0		
No. observations classified into crop type	Maize	0	0	22	0	0	0	4.50
% Classified into crop type		0	0	100	0	0		
No. observations classified into crop type	Rice	0	0	0	3	7	70	10
% Classified into crop type		0	0	0	30	70		
No. observations classified into crop type	Wheat	0	0	0	1	22	4.3	30.4
% Classified into crop type		0	0	0	4.35	95.65		
Tot Overall Error = 15.3%								
Overall Accuracy = 92%								

important Hyperion band to discriminate soybean varieties. Waveband 1982 (EMIR) corresponds to the reflectance postpeak 2 in MIR, which is sensitive to biomass, cellulose, and lignin.

The performance of hyperspectral data in discriminating crop types varied across the growing season depending on the growth stage of the crops. For instance, spectroradiometer reflectance data were able to discriminate cotton, maize, wheat, and rice in July but not in June when rice was in its early growing stage with sowing occurring in the last week of May (Cai et al., 2009) (see Table 4). Also, both in June and July, alfalfa was not discriminated from the above mentioned crops by spectroradiometer. Considering that in June alfalfa was in its senescence stage (harvest occurred in July), soil background might have affected the reflectance detected by the spectroradiometer at such a fine scale (0.1134 m). In May, Hyperion was able to discriminate maize from cotton (in several NIR, FNIR, and EMIR bands), and maize from wheat (in several NIR and FNIR bands); however, it could not distinguish cotton from wheat (and, likewise, all the three crops at the same time) probably because cotton was in its early growing stage with a high amount of soil background, and wheat was in its senescence stage with prevailing yellow pigments in its leaves and stems. On the other hands, both Hyperion and spectroradiometer significantly discriminated crop types when all were in their full growing stage. These results clearly imply the importance of timing in image acquisition for optimal crop discrimination and modeling. HyspIRI, with a revisit time of 19 days in the visible to short wave infrared (VSWIR: 380–2500 nm) (5 days in the mid and thermal infrared, TIR), should provide sufficient temporal coverage to enable accurate crop discrimination.

This study clearly identified the important as well as the redundant wavebands through: (1) principal component analysis (Table 5), and (2) very rigorous λ_1 (400–2500 nm) by λ_2 (400–2500 nm) contour plots (Figs. 3 to 6) involving 12,403 unique HVI model derived R-square values for each variable of each crop. These findings make significant contribution to data mining and in overcoming the Hughes' phenomenon. This is very valuable for future generations of satellites, such as the HyspIRI mission, which could either gather data from hundreds of hyperspectral narrowbands like Hyperion, from which users will have to extract appropriate optimal wavebands relevant for their application (*e.g.*, based on methods espoused in this paper), or, as an alternative, they could carry specialized optimal sensors with selective wavebands (*e.g.*, as reported for Hyperion in Table 6), focusing to gather data for targeted applications such as agriculture (Table 6) or vegetation. This will reduce data volume and optimize time and resources in image pre-processing, analysis, and interpretation.

Acknowledgments

The authors are thankful to NASA Science Mission Directorate's Earth Science Division for the research grant in response to NASA ROSES HyspIRI solicitation (NNH10ZDA001N-HYSPIRI).

References

Alchanatis, V., & Cohen, Y. (2011). Spectral and spatial methods for hyperspectral image analysis for estimation of biophysical and biochemical properties of agricultural crops. In P.S. Thenkabail, G. J. Lyon, & A. Huete (Eds.), *Hyperspectral remote sensing of vegetation* (pp. 239–308). Boca Raton, London, New York: CRC Press- Taylor and Francis Group.

Asner, G. P. (1998). Biophysical and biochemical sources of variability in canopy reflectance. *Remote Sensing of Environment*, *64*, 234–253.

Beckmann, T., & Mckinney, R. (2006). *Hyperion level 1GST (L1GST) product output files data format control book (DCFB)*. USGS Center for Earth Resource Observation and Science (EROS) (Volume: 1, Issue: April).

Berk, A., Anderson, G. P., Bernstein, L. S., Acharya, P. K., Dothe, H., Matthew, M. W., et al. (1999). MODTRAN4 radiative transfer modeling for atmospheric correction. *SPIE proceeding, optical spectroscopic techniques and instrumentation for atmospheric and space research III* (pp. 3756).

Boyd, D. S., & Ripple, W. J. (1997). Potential vegetation indices for determining global forest cover. *International Journal of Remote Sensing*, *18*, 395–1401.

Boyd, D. S., Wicks, T. E., & Curran, P. J. (1999). Use of middle infrared radiation to estimate the leaf area index of a boreal forest. *Tree Physiology*, *20*, 755–760.

Blackburn, G. A., & Ferwerda, J. G. (2008). Retrieval of chlorophyll concentration from leaf reflectance spectra using wavelet analysis. *Remote Sensing of Environment*, *112*, 1614–1632.

Bretscher, O. (1995). *Linear algebra with applications* (3rd ed.). Upper Saddle River NJ: Prentice Hall.

Cai, X., Thenkabail, P.S., Biradar, C. M., Platonov, A., Gumma, M., Dheeravath, V., et al. (2009). Water productivity mapping using remote sensing data of various resolutions to support "more crop per drop". *Journal of Applied Remote Sensing*, *3*, 033557. http://dx.doi.org/10.1117/1.3257643.

Chan, J. Cheung-Wai, & Paelinckx, D. (2008). Evaluation of random forest and adaboost tree-based ensemble classification and spectral band selection for ecotope mapping using airborne hyperspectral imagery. *Remote Sensing of Environment*, *112*, 2999–3011.

Chen, J., Wang, R., & Wang, C. (2008). A multiresolution spectral angle-based hyperspectral classification method. *International Journal of Remote Sensing*, *29*, 3159–3169.

Clevers, J. G. P. W., van der Heijden, G. W. A.M., Verzakov, S., & Schaepman, M. E. (2007). Estimating grassland biomass using SVM band shaving of hyperspectral data. *Photogrammetric Engineering and Remote Sensing*, *73*(10), 1141–1148.

Colombo, R., Busetto, L., Meroni, M., Rossini, M., & Panigada, C. (2011). Optical remote sensing of vegetation water content. In P.S. Thenkabail, G. J. Lyon, & A. Huete (Eds.), *Hyperspectral remote sensing of vegetation* (pp. 227). Boca Raton, London, New York: CRC Press- Taylor and Francis Group.

Congalton, R., & Green, K. (2009). *Assessing the accuracy of remotely sensed data: Principles and practices* (2nd ed.). Boca Raton, FL: CRC/Taylor & Francis.

Galvão, L. S., Roberts, D. A., Formaggio, A.R., Numata, I., & Breuni, F. M. (2009). View angle effects on the discrimination of soybean varieties and on the relationships between vegetation indices and yield using off-nadir Hyperion data. *Remote Sensing of Environment*, *113*, 846–856.

Geerken, R., Batikha, N., Celis, D., & DePauw, E. (2005). Differentiation of rangeland vegetation and assessment of its status: Field investigations and MODIS and SPOT VEGETATION data analyses. *International Journal of Remote Sensing*, *26*, 4499–4526. http://dx.doi.org/10.1080/01431160500213425.

Gitelson, A. (2011). Non-destructive estimation of foliar pigment (chlorophylls, carotenoids, and anthocyanins) contents: Evaluating a semi-analytical three-band model. In P.S. Thenkabail, G. J. Lyon, & A. Huete (Eds.), *Hyperspectral remote sensing of vegetation* (pp. 141–166). Boca Raton, London, New York: CRC Press- Taylor and Francis Group.

Gitelson, A. A., Gritz, Y., & Merzlyak, M. N. (2003). Relationships between leaf chlorophyll content and spectral reflectance and algorithms for non-destructive chlorophyll assessment in higher plant leaves. *Journal of Plant Physiology*, *160*, 271–282 (URL http://www.sciencedirect.com/science/article/pii/S0176161704704034).

Glahn, H. R. (1968). Canonical correlation and its relationship to discriminant analysis and multiple regression. *Journal of the Atmospheric Sciences*, *25*, 23–31.

Govender, M., Dye, P. J., Weiersbye, I. M., Witkowski, E. T. F., & Ahmed, F. (2009). Review of commonly used remote sensing and ground-based technologies to measure plant water stress. *WaterSA*, *35*, 741–752.

Hill, M. J. (2004). Grazing agriculture: Managed pasture, grassland, and rangeland. In S. L. Ustin (Ed.), *Manual of remote sensing. Remote sensing for natural resource management and environmental monitoring, Vol. 4*. (pp. 449–530). Hoboken, NJ: John Wiley & Sons.

Hocking, R. R. (1976). The analysis and selection of variables in linear regression. *Biometrics*, *3*, 1–49.

Houborg, R., & Boegh, E. (2008). Mapping leaf chlorophyll and leaf area index using inverse and forward canopy reflectance modelling and SPOT reflectance data. *Remote Sensing of Environment*, *112*, 186–202.

Jollineau, M. Y., & Howarth, P. J. (2008). Mapping an inland wetland complex using hyperspectral imagery. *International Journal of Remote Sensing*, *29*, 3609–3631.

Kalacska, M., & Sanchez-Azofeifa, G. A. (2008). *Hyperspectral remote sensing of tropical and sub-tropical forests*. Boca Raton, London, New York: CRC Press, Taylor and Francis Group, 352.

Lee, K. S., Cohen, W. B., Kennedy, R. E., Maiersperger, T. K., & Gower, S. T. (2004). Hyperspectral *versus* multispectral data for estimating leaf area index in four different biomes. *Remote Sensing of Environment*, *91*, 508–520.

Moran, M. S., Inoue, Y. E., & Barnes, M. (1997). Opportunities and limitations for image-based remote sensing in precision crop management. *Remote Sensing of Environment*, 19–346 (URL http://www.sciencedirect.com/science/article/pii/S003442579700045X).

National Aeronautics and Space Administration (NASA) (2013). Hyspiri mission study. California Institute of Technology. Available online at: http://hyspiri.jpl.nasa.gov/

Ollinger, S. V. (2011). Sources of variability in canopy reflectance and the convergent properties of plants. *The New Phytologist*, *189*, 375–394.

Pearson, K. (1901). On lines and planes of closest fit to systems of points in space. *Philosophical Magazine*, *2*(11), 559–572.

Pillai, K. C. S. (1955). Some new test criteria in multivariate analysis. *Annals of Mathematical Statistics*, 117–121 (26 pp.).

Rouse, J. W., Haas, R. H., Schell, J. A., & Deering, D. W. (1973). Monitoring vegetation systems in the Great Plains with ERTS'. *Third ERTS Symposium, NASA SP-351*, *I*, 309–317.

SAS Institute Inc. (2011). *SAS/STAT user's guide and software release, version 9.2*. Cary, NC: SAS Institute Inc.

Schaepman, M. E., Ustin, S. L., Plaza, A. J., Painter, T. H., Verrelst, J., & Liang, S. (2009). Earth system science related imaging spectroscopy—An assessment. *Remote Sensing of Environment*, *113*, 123–137.

Thenkabail, P.S. (2003). Biophysical and yield information for precision farming from near-real time and historical Landsat TM images. *International Journal of Remote Sensing*, *24*, 2879–2904.

Thenkabail, P.S., Enclona, E. A., Ashton, M. S., Legg, C., & Jean De Dieu, M. (2004). Hyperion, IKONOS, ALI, and ETM+ sensors in the study of African rainforests. *Remote Sensing of Environment*, *90*, 23–43.

Thenkabail, P.S., Enclona, E. A., Ashton, M. S., & Van Der Meer, V. (2004). Accuracy assessments of hyperspectral waveband performance for vegetation analysis applications. *Remote Sensing of Environment*, *91*, 354–376.

Thenkabail, P. S., Knox, J. W., Ozdogan, M., Gumma, M. K., Congalton, R., Wu, Z., You, S., Milesi, C., Finkral, A., Marshall, M., Mariotto, I., Giri, C., & Nagler, P. (2012). Assessing future risks to agricultural productivity, water resources and food security: how can remote sensing help? *Photogrammetric Engineering & Remote Sensing (PE&RS) Special Issue on Global Croplands*, *78*(8), 773–782.

Thenkabail, P.S., Lyon, G. J., & Huete, A. (2011). Advances in hyperspectral remote sensing of vegetation and agricultural crops. In P.S. Thenkabail, G. J. Lyon, & A. Huete (Eds.), *Hyperspectral remote sensing of vegetation* (pp. 3–29). Boca Raton, London, New York: CRC Press- Taylor and Francis Group.

Thenkabail, P.S., Smith, R. B., & De-Pauw, E. (2000). Hyperspectral vegetation indices and their relationships with agricultural crop characteristics. *Remote Sensing of Environment*, *71*, 158–182.

Thenkabail, P.S., Smith, R. B., & De-Pauw, E. (2002). Evaluation of narrowband and broadband vegetation indices for determining optimal hyperspectral wavebands for agricultural crop characterization. *Photogrammetric Engineering and Remote Sensing*, *68*, 607–621.

Varshney, P. K., & Arora, M. K. (2004). *Advanced image processing techniques for remotely sensed hyperspectral data*. Berlin, Germany: Springer.

Wilks, S. S. (1935). On the independence of *k* sets of normally distributed statistical variables. *Econometrika*, *3*, 309–326.